

Lamina Cribrosa Visibility Using Optical Coherence Tomography: Comparison of Devices and Effects of Image Enhancement Techniques

Michaël J. A. Girard,^{1,2} Tin A. Tun,² Rahat Husain,² Sanchalika Acharyya,³
Benjamin A. Haaland,^{3,4} Xin Wei,^{2,3} Jean M. Mari,⁶ Shamira A. Perera,² Mani Baskaran,²⁻⁴
Tin Aung,^{2,3,5} and Nicholas G. Strouthidis^{2,7,8}

¹In Vivo Biomechanics Laboratory, Department of Biomedical Engineering, National University of Singapore, Singapore

²Singapore Eye Research Institute, Singapore National Eye Centre, Singapore

³Centre for Quantitative Medicine, Duke-NUS Graduate Medical School, Singapore

⁴Department of Statistics and Applied Probability, National University of Singapore, Singapore

⁵Yong Loo Lin School of Medicine, National University of Singapore, Singapore

⁶Department of Medical Physics and Bioengineering, UCL, London, United Kingdom

⁷NIHR Biomedical Research Centre at Moorfields Eye Hospital NHS Foundation Trust and UCL Institute of Ophthalmology, London, United Kingdom

⁸Discipline of Clinical Ophthalmology and Eye Health, University of Sydney, Sydney, New South Wales, Australia

Correspondence: Nick G. Strouthidis, NIHR Biomedical Research Centre at Moorfields Eye Hospital NHS Foundation Trust and UCL Institute of Ophthalmology, 162 City Road, London EC1V 2PD, UK; nicholas.strouthidis@btinternet.com.

Submitted: May 29, 2014

Accepted: December 22, 2014

Citation: Girard MJA, Tun TA, Husain R, et al. Lamina cribrosa visibility using optical coherence tomography: comparison of devices and effects of image enhancement techniques. *Invest Ophthalmol Vis Sci*. 2015;56:865-874. DOI:10.1167/iov.14-14903

PURPOSE. To compare the visibility of the lamina cribrosa (LC) in optic disc images acquired from 60 glaucoma and 60 control subjects using three optical coherence tomography (OCT) devices, with and without enhanced depth imaging (EDI) and adaptive compensation (AC).

METHODS. A horizontal B-scan was acquired through the center of the disc using two spectral-domain (Spectralis and Cirrus; with and without EDI) and a swept-source (DRI) OCT. Adaptive compensation was applied post acquisition to improve image quality. To assess LC visibility, four masked observers graded the 1200 images in a randomized sequence. The anterior LC was graded from 0 to 4, the LC insertions from 0 to 2, and the posterior LC either 0 or 1. The effect of EDI, AC, glaucoma severity, and other clinical/demographic factors on LC visibility was assessed using generalized estimating equations.

RESULTS. The anterior LC was the most detectable feature, followed by the LC insertions. Adaptive compensation improved anterior LC visibility independent of EDI. Cirrus+EDI+AC generated the greatest anterior LC visibility grades (2.79/4). For LC insertions visibility, DRI+AC was the best method (1.10/2). Visibility of the posterior LC was consistently poor. Neither glaucoma severity nor clinical/demographic factors consistently affected LC visibility.

CONCLUSIONS. Adaptive compensation is superior to EDI in improving LC visibility. Visibility of the posterior LC remains poor suggesting impracticality in using LC thickness as a glaucoma biomarker.

Keywords: glaucoma, lamina cribrosa, optical coherence tomography, enhanced depth imaging, adaptive compensation, intraocular pressure

The lamina cribrosa (LC) is a porous connective tissue structure within the optic nerve head (ONH) and is regarded as a major site of irreversible damage to the retinal ganglion cell axons in glaucoma.¹ The LC has recently become detectable in vivo following improvements to the axial resolution, depth penetration, and scanning speeds of optical coherence tomography (OCT) imaging.² There is broad scientific interest in pursuing in vivo imaging of the LC to generate parameters (structural or biomechanical) that may serve as biomarkers for glaucomatous damage or risk of future visual loss.^{3,4} There has been a recent plethora of research articles devoted to OCT imaging of the LC in both healthy and glaucoma subjects, predominantly using commercially available devices. These studies have examined LC microstructure,⁵ thickness,⁶ central ridge shape,⁷ focal defects,⁸ movements, and displacements induced by the IOP,^{9,10} IOP-induced strains,^{11,12} depth,¹³

and curvature.¹⁴ These papers all indicate that in vivo LC imaging shows promise in establishing novel glaucoma biomarkers.

One potential barrier to the development of LC imaging for clinical glaucoma is the clinical observation that 'deep' OCT images of the ONH are often of variable quality, and the presence of an LC signal is not always consistent or indeed convincing. This is largely due to light-attenuation artefacts,¹⁵ such as vessel shadowing and fading of the signal with increasing depth. Optical coherence tomography images of the LC are therefore less informative than those acquired using gold standard ex vivo techniques, such as conventional histology,¹⁶ three-dimensional (3D) histomorphometry¹⁷ and second harmonic generation imaging.¹⁸ While there is a credible degree of fidelity between OCT images and histology of the LC,¹⁹ at least for the anterior LC surface, variability of LC detection by OCT limits the wider applicability of in vivo LC

imaging and may prevent translation of this technologic advance into clinical practice.

Recent developments in OCT hardware, such as enhanced depth imaging (EDI),²⁰ and in OCT light-attenuation correction software such as adaptive compensation²¹ (AC) have been reported to significantly improve the visibility of the LC without compromising acquisition time. The benefits of either EDI or AC, or a combination of both, in terms of LC visibility have yet to be established over multiple OCT platforms.

The aim of this study was to assess the visibility of the LC using three commercially available OCT devices and to investigate the effect of AC, EDI, or the two combined on LC visibility.

METHODS

Patient Recruitment

This study was a cross-sectional, observational study of both glaucoma and healthy individuals attending the Singapore National Eye Centre, Singapore. All participants gave written informed consent. The study adhered to the tenets of the Declaration of Helsinki and was approved by the institutional review board of the hospital. Inclusion criteria for healthy controls ($n = 60$) were: IOP less than or equal to 21 mm Hg, healthy optic nerves with vertical cup disc ratio (CDR) less than or equal to 0.5 and normal visual fields. We recruited POAG ($n = 28$), normal-tension glaucoma (NTG; $n = 13$), and primary-angle closure glaucoma (PACG; $n = 19$) subjects. POAG was defined as glaucomatous optic neuropathy (GON; characterized as loss of neuroretinal rim with vertical CDR > 0.7 and/or focal notching with nerve fibre layer defect attributable to glaucoma and/or asymmetry of CDR between eyes > 0.2) with repeatable glaucomatous visual field defects with raised IOP greater than or equal to 21 mm Hg in at least one eye. Normal-tension glaucoma was defined as GON with repeatable glaucomatous visual field defects with IOP less than or equal to 21 mm Hg on diurnal testing, in at least one eye. Primary-angle closure glaucoma was defined as the presence of GON with compatible visual field loss, in association with a closed anterior chamber angle and raised IOP greater than or equal to 21 mm Hg and/or peripheral anterior synechiae in at least one eye. A closed anterior chamber angle was defined as the posterior trabecular meshwork not being visible in at least 180° of anterior chamber angle.

After taking medical and demographic history, all participants underwent the following examinations: measurement of visual acuity, axial length and central anterior chamber depth measurement (both using IOL_{Master}; Carl Zeiss Meditec, Dublin, CA, USA), slit-lamp biomicroscopy, IOP measurement with Goldmann applanation tonometry, standard automated perimetry (Humphrey Visual Field Analyzer II; Carl Zeiss Meditec), and OCT imaging with three modalities after pupillary dilatation with tropicamide 1% on the same day. All PACG subjects had patent peripheral iridotomies and IOP was checked post dilation to ensure that there had been no clinically significant spiking of IOP.

Subjects with any corneal abnormalities that would preclude reliable imaging were excluded from the study. The staging/severity of functional damage (visual field loss) in the glaucomatous eyes was categorized by the Hodapp-Parrish-Anderson (H-P-A) system, the details of which have been reported elsewhere.²²

Optical Coherence Tomography Imaging

After dilatation with tropicamide 1%, OCT imaging was performed on seated subjects under dark room conditions.

Images were acquired by a single operator (TAT), masked to diagnosis, with the right ONH being imaged in all subjects, unless the inclusion criteria were met only in the left eye, in which case the left eye was imaged. A horizontal B-scan (0°) was acquired through the centre of the ONH of all subjects using three commercially-available OCT devices. The devices were two spectral-domain (SD) OCT units and one swept source (SS) OCT unit. Five images were acquired in total for each ONH: one standard acquisition and one EDI acquisition for each of the two SD-OCT devices and one non-EDI standard acquisition for the SS-OCT (EDI functionality not available on this device).

Spectral-Domain Optical Coherence Tomography. The SD-OCT devices utilized were the Cirrus (model 4000; Carl Zeiss Meditec) and the Spectralis (Heidelberg Engineering, Heidelberg, Germany). The single line scan width of Cirrus OCT was 6 mm with 20 B-scans averaging while that of Spectralis OCT was 8.9 mm with 48 B-scans averaging. The intention was to establish a consistent averaging number between the three devices; $n = 20$ was the Cirrus setting closest to the $n = 48$ available for both the Spectralis and the SS-OCT unit.

Swept-Source Optical Coherence Tomography. Swept-source OCT uses a tunable laser as a light source at 1050-nm wavelength to provide a scanning speed of 100,000 A-scans per second with an axial resolution of $8 \mu\text{m}$.²³ In this study, we used the Deep Range Imaging (DRI) OCT (Atlantis; Topcon, Tokyo, Japan). A single-line-scanning protocol of DRI was used and the scan width was 6 mm with 48 B-scans averaging.

Light Attenuation Correction Using Adaptive Compensation

In order to remove the deleterious effects of light attenuation in OCT images, all horizontal B-scans were post processed using AC.^{15,21} Adaptive compensation has been demonstrated to remove blood vessel shadows in ONH OCT images, improve the visibility of the anterior LC surface, improve the visibility of LC/scleral insertions and focal LC defects, and help in identifying the posterior LC surface in small groups of patients.^{3,15,21,24} In AC, a threshold exponent is used to remove the effects of noise over-amplification at high depth, thus facilitating posterior LC surface detection. Threshold exponents were chosen independently for each OCT device and were 1 (Cirrus), 14 (Spectralis), and 11 (DRI). The threshold exponent indicates the image depth (higher exponent = higher depth) at which compensation is stopped to limit the effects of noise over-amplification. Note that the threshold exponent is by nature machine-specific because data may be acquired and processed differently from one device to another. To this end, all images were reviewed manually (MJAG, masked to diagnosis) to ensure the selected threshold exponents did not compromise the visibility of the LC for each device. A compensation contrast exponent of 2 was also selected for all images.¹⁵ All standard and EDI acquisitions (processed with and without AC) are shown for the same patient using all three devices in Figure 1.

Lamina Cribrosa Visibility Grading

A subjective grading system was designed to assess the degree of visibility of the anterior LC surface, the LC insertions into the sclera, and the posterior LC surface. Four expert observers (NGS, MJAG, SP, and RH) each reviewed the 1200 images (5 noncompensated + 5 compensated images for each of 120 ONHs) in a randomized sequence, masked to the diagnosis, to the type of device and the imaging technique (non-EDI/EDI/

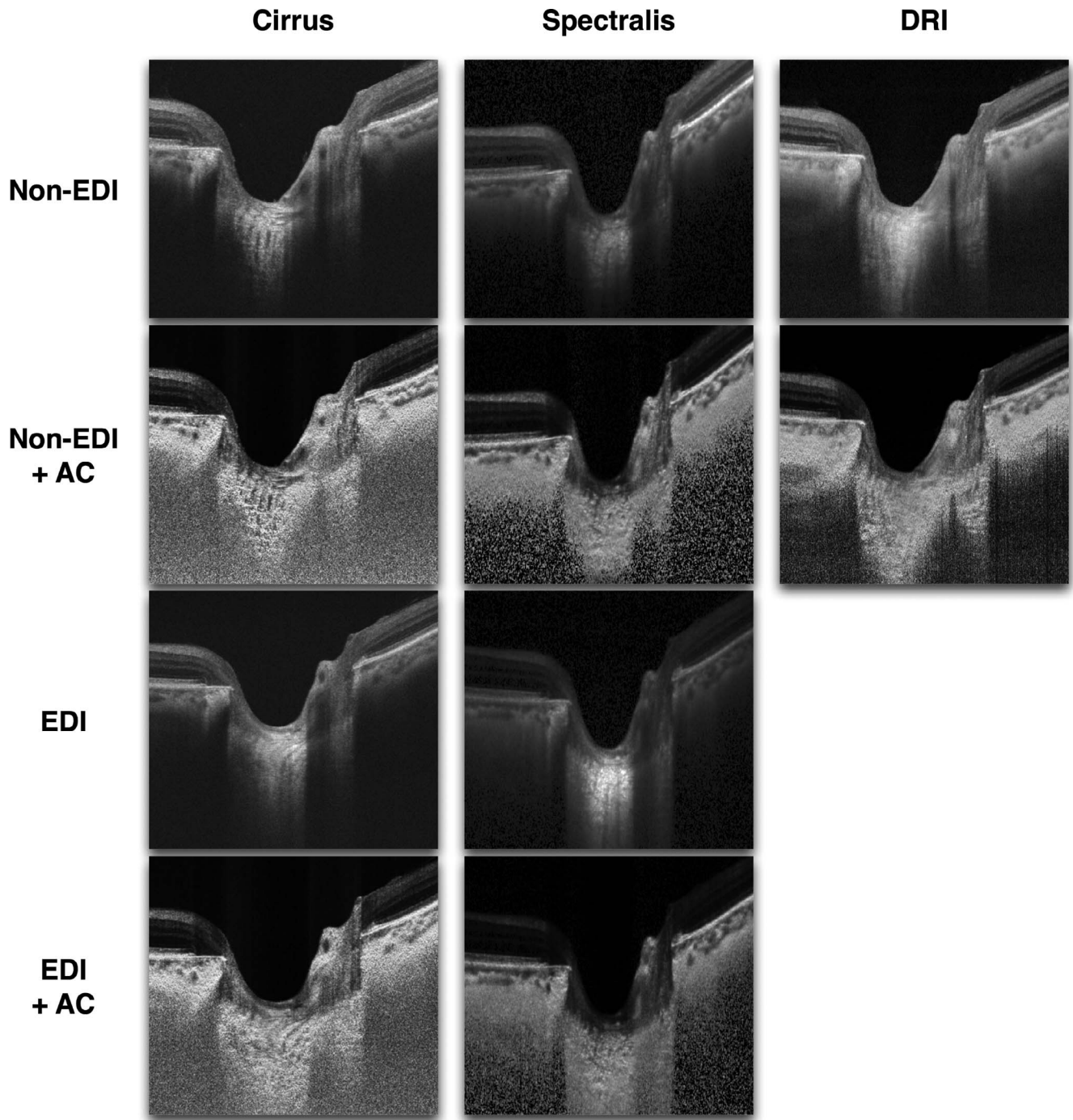


FIGURE 1. Each ONH was imaged five times (single horizontal B-Scan) using Cirrus (with and without EDI), Spectralis (with and without EDI), and DRI OCT. All images were then post processed with AC in order to improve contrast and deep-tissue visibility. This process resulted in 10 images per patient (shown here for one selected patient) and repeated for 120 patients resulting in a total of 1200 images that were subjected to manual grading.

non-AC/AC). Each observer ascribed Bruch's membrane opening (BMO) points on either side of the optic disc in each B-scan using custom-written JAVA code in ImageJ software (<http://imagej.nih.gov/ij/>; provided in the public domain by the National Institutes of Health, Bethesda, MD, USA)²⁵ that demarcated the 25%, 50%, and 75% distances within the horizontal length between the two BMO points (Fig. 2). The anterior LC was graded as 0 if no part of it was visible between the two BMO points, 1 if less than 25% of the width was

visible, 2 for 25% to 50%, 3 for 50% to 75%, and 4 for greater than 75%. The lamellar insertion visibility was graded 0 if neither insertion into the sclera was visible, 1 if only one insertion was visible and 2 if both insertions were visible. The posterior LC was graded either 0, if none of it was visible between the two BMO points, or 1, if the observer could convincingly identify any portion of the posterior surface between the two BMO points.

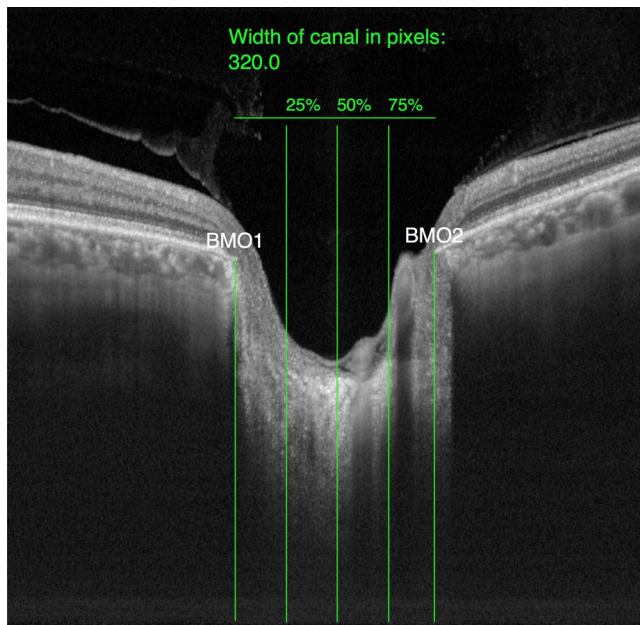


FIGURE 2. Subjective grading scheme for LC visibility. For each ONH B-scan (with and without EDI or AC), each grader marked the two points of Bruch's membrane opening on either side of the optic disc (indicated as BMO1 and BMO2). The distance between BMO1 and BMO2 was split equally into four subregions. The anterior LC was graded as 0 if it was not visible at all between the two BMO points, 1 if less than 25% of the width was visible, 2 for 25% to 50%, 3 for 50% to 75% and 4 for greater than 75%. In the figure shown, the anterior LC visibility grade is 4 as the anterior LC signal is visible in 4 subregions. The LC visibility grade is 0 as neither LC insertion is visible and the posterior LC visibility grade is 0 as no part of the posterior LC is visible.

Statistical Analysis

Demographic and clinicopathological characteristics of glaucoma subjects and healthy controls were compared using χ^2 and *t*-tests for categorical and continuous variables, respectively. The mean visibility grade with 95% confidence intervals (CIs) was estimated for each method and for each LC region of interest, in the context of a generalized estimating equation (GEE) model with an identity link function (for anterior LC and LC insertions visibility) or a logistic link function (for posterior LC visibility). The mean visibility grade was compared between methods using Wald tests. For posterior LC visibility, odds ratios (OR) were calculated comparing the visibility scores for each method. The same GEE approach with a fixed effect for grader was adopted to identify the influence of demographic and clinical features on LC visibility and to determine the association between degree of glaucoma severity (used as a continuous variable) and LC visibility.

Anterior LC and LC insertion visibility agreement among the four expert observers was assessed using Fleiss' kappa statistics. All statistical analyses were performed using the R 3.0.1 software (R Development Core Team; in the public domain, <http://www.r-project.org/>, 2012).

RESULTS

Demographic and clinical characteristics for all 120 subjects tested are summarized in Table 1.

Effects of EDI and AC on Anterior LC Visibility

We found that EDI improved the visibility of the anterior LC surface boundary for both Cirrus (mean score increase: +0.16;

$P = 0.02$) and Spectralis (mean score increase: +0.52; $P < 0.001$) with no evidence of a difference between the two devices after application of EDI (+0.06; $P = 0.51$; Table 2; Fig. 3A). Similarly, AC improved anterior LC visibility for both Cirrus (+1.09; $P < 0.001$) and Spectralis (+1.21; $P < 0.001$), with Cirrus+AC outperforming Spectralis+AC (+0.18; $P = 0.039$). Application of AC outperformed the improvement in anterior lamina visibility achieved by EDI alone (+0.93 for Cirrus and +0.69 for Spectralis; $P < 0.001$). Overall, combining AC with EDI resulted in the best mean anterior LC visibility grades (2.79/4 for Cirrus and 2.67/4 for Spectralis) with Cirrus+EDI+AC performing as well as Spectralis+EDI+AC ($P = 0.21$).

We found that DRI outperformed Cirrus (+0.30; $P = 0.002$), and Spectralis (+0.61; $P < 0.001$); performed as well as Cirrus+EDI (+0.14; $P = 0.12$) and Spectralis+EDI (+0.08; $P = 0.38$), but was outperformed by Cirrus+AC (−0.79; $P < 0.001$) and Spectralis+AC (−0.60; $P < 0.001$). Applying AC to DRI images resulted in an increase in mean anterior LC visibility grade (+0.92; $P < 0.001$). Overall, DRI+AC outperformed all imaging combinations, but not Cirrus+EDI+AC (−0.03; $P = 0.68$), Cirrus+AC (+0.13; $P = 0.17$), and Spectralis+EDI+AC (+0.08; $P = 0.39$) for which performance was comparable.

Effects of EDI and AC on LC Insertion Visibility

We found that EDI improved the visibility of LC insertion for both Cirrus (mean score increase: +0.10; $P = 0.002$) and Spectralis (mean score increase: +0.13; $P < 0.001$) with no evidence of a difference between the two devices after application of EDI (+0.02; $P = 0.61$; Table 3; Fig. 3B). Similarly, AC improved LC insertion visibility grade for both Cirrus (+0.56; $P < 0.001$) and Spectralis (+0.53; $P < 0.001$), with no evidence of a difference between the two devices after application of AC (0.04; $P = 0.37$). Improvements in LC insertion visibility due to AC were greater than those from EDI alone (+0.46 for Cirrus and +0.40 for Spectralis; $P < 0.001$ for both). Overall, combining AC with EDI resulted in the highest mean LC insertion visibility grades (0.92/2 for Cirrus and 1.02/2 for Spectralis) with Spectralis+EDI+AC outperforming Cirrus+EDI+AC (+0.10; $P = 0.032$). Interestingly, Cirrus+EDI+AC and Cirrus+AC performed equally well (0; $P = 1.0$).

We found that DRI outperformed Cirrus (+0.15; $P < 0.001$) and Spectralis (+0.16; $P < 0.001$). It performed similarly to Cirrus+EDI (+0.05; $P = 0.21$) and Spectralis+EDI (+0.02; $P = 0.52$), but was outperformed by Cirrus+AC and Spectralis+AC (−0.41 and −0.37, respectively; $P < 0.001$ for both). Applying AC to DRI images resulted in an increase in mean LC insertion visibility grade (+0.59; $P < 0.001$). Overall, DRI+AC outperformed all imaging combinations, including Cirrus+EDI+AC (+0.18; $P < 0.001$), but not Spectralis+EDI+AC (+0.08; $P = 0.11$) for which performance was comparable.

Posterior LC Boundary Visibility

Overall, posterior LC visibility grades were low, and this was true for all devices and techniques (Fig. 3C). Spectralis+AC had the highest probability to achieve posterior LC visibility (0.357) followed by Cirrus+AC (0.254). We found evidence that EDI increased the visibility of the posterior LC boundary for Spectralis ($P = 0.027$) but not for Cirrus ($P = 0.094$), while AC did for both (all $P < 0.001$). Combining EDI with AC increased the posterior LC visibility for Cirrus (OR: 1.88; $P = 0.001$) and Spectralis (OR: 2.1; $P < 0.001$), although Spectralis+AC provided better performance than Spectralis+EDI+AC (OR: 1.88; $P = 0.001$) and Cirrus+AC performed as well as Cirrus+EDI+AC ($P = 0.61$).

TABLE 1. Demographic and Clinical Characteristics of 120 Study Subjects

Demographics and Clinical Characteristics	Overall Population, N, %	Visually Healthy Subjects, n = 60	Subjects With Glaucoma, n = 60	P Value
Sex				
Male	62 (51.7)	28 (46.7)	34 (56.7)	0.361
Female	58 (48.3)	32 (53.3)	26 (43.3)	
Age, y				
Mean (SD)	63.64 (10.79)	60.98 (9.09)	66.3 (11.74)	0.006
Median (range)	63.92 (27.8–86.1)	61.3 (38.4–79.6)	66.8 (27.8–86.1)	
Ethnicity				
Chinese	102 (85.0)	49 (81.7)	53 (88.3)	0.443
Non-Chinese	18 (15.0)	11 (18.3)	7 (11.7)	
IOP, mm Hg				
Mean (SD)	20.06 (7.04)	16.07 (3.04)	23.98 (7.64)	<0.001
Median (range)	19 (10–52)	16.0 (10–21)	22.5 (14–52)	
Severity of glaucoma (N = 60)				
Early (MD < –6 dB)	20 (33.3)		20 (33.3)	
Moderate (MD –6 to –12 dB)	21 (35.0)		21 (35.0)	
Late (MD > –12 dB)	19 (31.7)		19 (31.7)	
Axial length, mm				
Mean (SD)	23.9 (1.3)	24.11 (1.23)	23.69 (1.35)	0.089
Median (range)	23.6 (21.43–27.62)	23.97 (22.09–27.06)	23.34 (21.43–27.62)	
Lens status				
Phakic	93 (77.5)	52 (86.7)	41 (68.3)	0.029
Pseudophakic	27 (22.5)	8 (13.3)	19 (31.7)	
Anterior chamber depth in mm				
Mean (SD)	3.4 (0.70)	3.46 (0.59)	3.34 (0.79)	0.367
Median (range)	3.4 (2.13–5.23)	3.41 (2.28–5.23)	3.19 (2.13–5.16)	

P values comparing glaucoma subjects and visually healthy controls are from χ^2 tests for categorical variables and *t*-tests for continuous variables.

We found that DRI had a higher probability of detecting the posterior LC boundary when compared with Spectralis (OR: 2.35; $P < 0.001$) and Cirrus (OR: 1.59; $P = 0.022$). The application of AC to DRI images did not significantly increase the probability of visualizing the posterior LC boundary ($P = 0.76$).

On average, and for the techniques that used AC, the posterior LC boundary was only visible in 21.0% (Spectralis+AC), 16.9% (Cirrus+AC), 15.6% (Cirrus+EDI+AC), 12.9% (DRI+AC), and in 12.3% (Spectralis+EDI+AC) of patients. For the techniques that did not use AC, the posterior LC boundary was only visible in 13.5% (DRI), 11.9% (Cirrus+EDI), 9.6%

(Spectralis+EDI), 9.0% (Cirrus), and in 6.3% (Spectralis) of patients.

Because of the small number of eyes in which the posterior LC boundary was visible, no further statistical analysis could reasonably be performed on the posterior LC boundary. The following sections only report results related to anterior LC boundary and LC insertion visibility.

Agreement Among Expert Observers

We found slight to fair levels of agreement among the four expert observers in their anterior LC visibility grades with

TABLE 2. Multiple Pair-Wise Comparisons of the Devices Employed to Measure Anterior LC Surface Visibility

	Cirrus	Cirrus+ EDI	Cirrus+ AC	Cirrus+ EDI+AC	Spectralis	Spectralis+ EDI	Spectralis+ AC	Spectralis+ EDI+AC	DRI	DRI+ AC
Cirrus										
Cirrus+EDI	0.16*									
Cirrus+AC	1.09‡	0.93‡								
Cirrus+EDI+AC	1.26‡	1.10‡	0.17*							
Spectralis	<i>–0.31‡</i>	<i>–0.46‡</i>	<i>–1.39‡</i>	<i>–1.56‡</i>						
Spectralis+EDI	0.22*	0.06	<i>–0.87‡</i>	<i>–1.04‡</i>	0.52‡					
Spectralis+AC	0.91‡	0.75‡	<i>–0.18*</i>	<i>–0.35‡</i>	1.21‡	0.69‡				
Spectralis+EDI+AC	1.14‡	0.98‡	0.05	<i>–0.12</i>	1.45‡	0.93‡	0.23*			
DRI	0.30‡	0.14	<i>–0.79‡</i>	<i>–0.96‡</i>	0.61‡	0.08	<i>–0.60‡</i>	<i>–0.84‡</i>		
DRI+AC	1.22‡	1.06‡	0.13	<i>–0.03</i>	1.53‡	1.01‡	0.32‡	0.08	0.92‡	

Bolded values indicate that the device in the left column performs better than that in the first row, and italic the inverse. Mean visibility scores comparing two methods; * $P < 0.05$, † $P < 0.01$, ‡ $P < 0.001$.

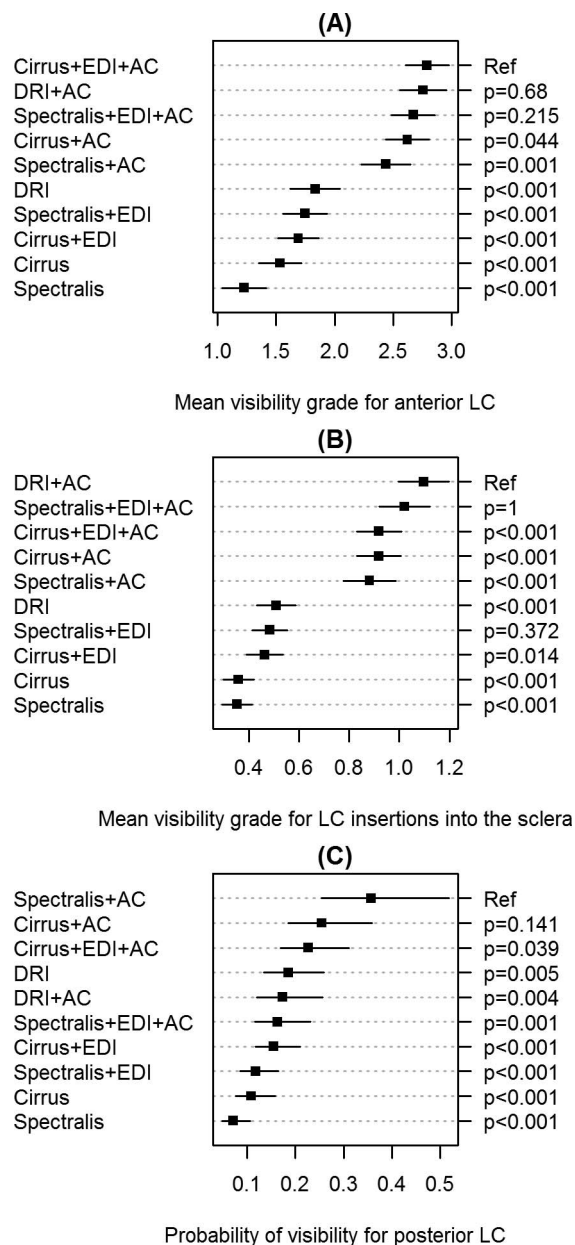


FIGURE 3. Mean visibility grades with 95% CIs for (A) the anterior LC surface and (B) the LC insertions into the sclera. (C) Probability with 95% confidence limits of visibility for posterior LC surface. Corresponding *P* values comparing each method with the best performing method are shown on the right of each graph.

Fleiss' κ ranging from 0.19 to 0.31 for all devices and methods. Agreement was found to decrease with performance for Spectralis and DRI (from 0.31 [Spectralis] to 0.19 [Spectralis+EDI+AC]; from 0.26 [DRI] to 0.20 [DRI+AC]), and to increase with performance for Cirrus (from 0.21 [Cirrus] to 0.24 [Cirrus+EDI+AC]).

Slight to fair levels of agreement were found among the four expert observers as regards their LC insertion visibility grades with Fleiss' κ ranging from 0.08 to 0.32. For this parameter, agreement increased with performance for all three devices: from 0.08 (Spectralis) to 0.22 (Spectralis+EDI+AC), from 0.13 (Cirrus) to 0.20 (Cirrus+EDI+AC), and from 0.20 (DRI) to 0.23 (DRI+AC).

Demographic and Clinical Factors Affecting LC Visibility

The effect of demographic and clinical factors on LC visibility was inconsistent across all imaging and enhancement techniques. No demographic/clinical factors had a consistent negative impact on anterior LC and LC insertion visibility (Table 4; using statistical significance at the 0.05 level).

Association Between Degree of Glaucoma Severity and LC Visibility

We found no evidence of association between glaucoma severity (described as a continuous variable) and LC insertion visibility (all $P > 0.114$; Table 5). Decreased anterior LC visibility was associated with increased glaucoma severity in a single isolated case (i.e., when Cirrus+EDI was used).

DISCUSSION

This study establishes the performance of three commercially available OCT devices in detecting features of the LC in vivo in human subjects. Furthermore, this study has demonstrated the effect of EDI and/or AC on the visibility of these LC parameters. These results reflect the validity and consistency of in vivo LC images captured with current techniques. The implication is that not all LC features are sufficiently visible to be used in clinical glaucoma management.

We found that for SD-OCT devices (Cirrus and Spectralis), EDI was able to improve the visibility of the anterior LC surface and the LC insertions, which is consistent with previous SD-OCT studies in humans^{26,27} and monkeys.²⁸ However, these improvements were lower than those obtained with AC. For these two features, SD-OCT devices achieved their best performance when EDI and AC were combined, although there was little evidence that Cirrus+EDI+AC differed from Cirrus+AC for LC insertions, indicating the limited additional benefit of EDI on LC visibility.

For all devices, AC outperformed all standard and EDI acquisitions for both anterior LC and LC insertion visibility. The best mean visibility grades for the LC insertions was provided by DRI+AC and the second-best mean visibility grades for the anterior LC boundary. This was unsurprising as DRI is an SS-OCT device with a higher wavelength light source (1050 nm), allowing for deeper signal penetration. While a previous study reported that LC visibility was not improved with 1050-nm SS-OCT relative to 860 SD-OCT,²⁹ 1050-nm SS-OCT is still more likely to capture deeper faint signals. Even if such signals are weak in the original images, and thus invisible to the naked eye, they would be amplified by postprocessing techniques such as AC, explaining the improvements in LC visibility we observed.

In all cases, we found that the posterior LC boundary was poorly detected even with the help of EDI and/or AC. In fact, AC improved posterior LC visibility inconsistently, with improvements observed for Cirrus and Spectralis but not for DRI. Using the best-performing imaging combination (Spectralis+AC), the posterior LC boundary was only detectable in 21% of the imaged patients. This was reduced to 13.5% for the best technique that did not employ AC (DRI). This observation is critical as it questions the feasibility of reliably measuring LC thickness. Recent studies have reported that LC thickness was decreased in NTG patients⁶ (with and without disc hemorrhages), and that the diagnostic ability of LC thickness in patients with glaucoma was comparable or better than that of peripapillary retinal nerve fibre layer thickness.³⁰ Other studies found a significant increase in LC thickness with age³¹ and

TABLE 3. Multiple Pair-Wise Comparisons of the Devices Employed to Measure LC Insertion Visibility

	Cirrus	Cirrus+ EDI	Cirrus+ AC	Cirrus+ EDI+AC	Spectralis	Spectralis+ EDI	Spectralis+ AC	Spectralis+ EDI+AC	DRI	DRI+ AC
Cirrus										
Cirrus+EDI	0.10†									
Cirrus+AC	0.56‡	0.46‡								
Cirrus+EDI+AC	0.56‡	0.45‡	0.00							
Spectralis	<i>-0.006</i>	<i>-0.11‡</i>	<i>-0.57‡</i>	<i>-0.57‡</i>						
Spectralis+EDI	0.12†	0.02	<i>-0.43‡</i>	<i>-0.43‡</i>	0.13‡					
Spectralis+AC	0.52‡	0.42‡	<i>-0.04</i>	<i>-0.04</i>	0.53‡	0.40‡				
Spectralis+EDI+AC	0.66‡	0.55‡	0.10*	0.10*	0.67‡	0.54‡	0.14†			
DRI	0.15‡	0.05	<i>-0.41‡</i>	<i>-0.41‡</i>	0.16‡	0.02	<i>-0.37‡</i>	<i>-0.51‡</i>		
DRI+AC	0.74‡	0.63‡	0.18‡	0.18‡	0.75‡	0.61‡	0.22‡	0.08	0.59‡	

Bolded values indicate that the device in the left column performs better than that in the first row, and italic the inverse. Mean visibility scores comparing two methods; * $P < 0.05$, † $P < 0.01$, ‡ $P < 0.001$.

following trabeculectomy at 6 months post surgery.⁹ Likewise significantly thinner LC was observed in eyes with pseudoexfoliation as compared with POAG eyes.³² The majority of these studies were performed in Korean cohorts and most used EDI (but not AC) to improve visibility. It is possible that LC may have been more visible in those populations, or the scanning protocols were optimized to capture the posterior surface. In terms of scan acquisition, it is possible that some images may have been acquired at a depth where the signal from the posterior optic nerve was too high, thereby losing the contrast between the posterior lamellar zone and the retrolamellar region. Furthermore, in such cases the application of AC will further enhance the high signal in the posterior optic nerve thereby compounding the loss of contrast. For example, our ability to detect the posterior surface may be limited by the fact that we were only using a single line scan, rather than a 3D raster volume. It is possible that in some eyes a ‘central ridge’ may be present in the lamina, reducing the visibility of the LC

in the central line scan. With the 3D raster scan pattern, one can view multiple successive B-scans within a volume to look for consistent visual clues that may help to identify the posterior lamellar surface. Techniques such as maximum intensity projection^{33,34} exploit the availability of serial scans within a volume to facilitate posterior surface visualization. Our results indicate that OCT measurement of LC thickness may not be a feasible clinical option, at least in this predominantly ethnic Chinese population and using the scan acquisition protocols adopted by this study.

In all but one isolated circumstance, we found no association between glaucoma severity and the visibility of the anterior LC boundary, and of the LC insertions. One might reasonably have expected a decreased LC visibility with glaucoma, since glaucomatous ONHs have deeper cups and are affected by collagen remodelling in early³⁵ and moderate/severe glaucoma stages,³⁶ by outward LC migration, by collagen cross-linking and elastin degradation with age, which

TABLE 4. Estimates of Mean Difference in Visibility Grades (P Values) From Univariate Analysis of Demographic and Clinical Characteristics Associated With the Measures of Lamellar Visibility

Variates*	Cirrus	Cirrus+EDI	Cirrus+AC	Cirrus+ EDI+AC	Spectralis
Anterior LC visibility					
Age	0.01 ($P = 0.149$)	0 ($P = 0.77$)	0 ($P = 0.632$)	0 ($P = 0.721$)	0.01 ($P = 0.548$)
Sex	-0.11 ($P = 0.574$)	0.03 ($P = 0.874$)	0.04 ($P = 0.836$)	0.02 ($P = 0.92$)	0.1 ($P = 0.617$)
Ethnicity	0.07 ($P = 0.805$)	-0.07 ($P = 0.805$)	0 ($P = 0.999$)	0.12 ($P = 0.69$)	0.05 ($P = 0.829$)
Diagnosis of glaucoma	-0.47 ($P = 0.017$)	-0.53 ($P = 0.004$)	-0.2 ($P = 0.313$)	-0.23 ($P = 0.251$)	-0.25 ($P = 0.235$)
Eye	0.05 ($P = 0.901$)	0.16 ($P = 0.672$)	-0.26 ($P = 0.544$)	0.12 ($P = 0.669$)	-0.12 ($P = 0.768$)
IOP	-0.01 ($P = 0.479$)	-0.01 ($P = 0.667$)	-0.02 ($P = 0.164$)	-0.01 ($P = 0.563$)	-0.02 ($P = 0.142$)
Axial length	-0.04 ($P = 0.56$)	-0.09 ($P = 0.223$)	-0.19 ($P = 0.015$)	-0.18 ($P = 0.006$)	-0.05 ($P = 0.558$)
ACD	0.03 ($P = 0.837$)	-0.07 ($P = 0.667$)	-0.04 ($P = 0.794$)	-0.05 ($P = 0.68$)	-0.24 ($P = 0.114$)
Lens status	0.29 ($P = 0.277$)	-0.01 ($P = 0.967$)	0.14 ($P = 0.521$)	0.26 ($P = 0.212$)	-0.39 ($P = 0.113$)
LC insertion visibility					
Age	0.01 ($P = 0.143$)	0 ($P = 0.492$)	0.01 ($P = 0.041$)	0 ($P = 0.692$)	0 ($P = 0.265$)
Sex	0.03 ($P = 0.694$)	0.03 ($P = 0.673$)	-0.01 ($P = 0.902$)	0.02 ($P = 0.834$)	0.09 ($P = 0.163$)
Ethnicity	0.04 ($P = 0.633$)	-0.07 ($P = 0.503$)	-0.01 ($P = 0.959$)	0.04 ($P = 0.738$)	-0.11 ($P = 0.134$)
Diagnosis of glaucoma	-0.15 ($P = 0.02$)	-0.13 ($P = 0.098$)	-0.08 ($P = 0.417$)	-0.02 ($P = 0.858$)	-0.07 ($P = 0.309$)
Eye	-0.05 ($P = 0.696$)	0.04 ($P = 0.785$)	0.01 ($P = 0.971$)	0.01 ($P = 0.917$)	-0.07 ($P = 0.586$)
IOP	0 ($P = 0.261$)	-0.01 ($P = 0.129$)	-0.01 ($P = 0.028$)	-0.01 ($P = 0.336$)	0 ($P = 0.181$)
Axial length	0.02 ($P = 0.48$)	0.01 ($P = 0.809$)	-0.09 ($P = 0.006$)	-0.07 ($P = 0.024$)	-0.02 ($P = 0.371$)
ACD	0 ($P = 0.954$)	-0.06 ($P = 0.372$)	-0.11 ($P = 0.178$)	-0.01 ($P = 0.903$)	-0.03 ($P = 0.619$)
Lens status	0.09 ($P = 0.355$)	0.01 ($P = 0.938$)	0.02 ($P = 0.863$)	0.05 ($P = 0.708$)	-0.05 ($P = 0.58$)

Statistical significance ($P < 0.05$) is highlighted in bold. ACD, anterior chamber depth.

* Lens status refers to a comparison of pseudophakic versus phakic subjects. For sex, the comparison was of female versus male subjects. For ethnicity, the comparison was non-Chinese versus Chinese. For diagnosis, the comparison was healthy versus glaucoma subjects. For eye, it was for left versus right. For all others, it was for one unit change in the value of the predictor.

TABLE 5. Univariate Analysis of Glaucoma Severity, as a Continuous Variable, in Association With the Measures of LC Visibility

Devices	Anterior LC Visibility	LC Insertion Visibility
Cirrus	-0.02 (<i>P</i> = 0.053)	-0.01 (<i>P</i> = 0.114)
Cirrus+EDI	-0.03 (<i>P</i> = 0.004)	-0.005 (<i>P</i> = 0.279)
Cirrus+AC	-0.02 (<i>P</i> = 0.285)	-0.002 (<i>P</i> = 0.782)
Cirrus+EDI+AC	-0.01 (<i>P</i> = 0.465)	-0.01 (<i>P</i> = 0.329)
Spectralis	-0.01 (<i>P</i> = 0.633)	-0.002 (<i>P</i> = 0.613)
Spectralis+EDI	-0.01 (<i>P</i> = 0.604)	0.005 (<i>P</i> = 0.274)
Spectralis+AC	-0.01 (<i>P</i> = 0.491)	-0.003 (<i>P</i> = 0.7)
Spectralis+EDI+AC	-0.004 (<i>P</i> = 0.705)	0.001 (<i>P</i> = 0.898)
DRI	-0.02 (<i>P</i> = 0.201)	-0.005 (<i>P</i> = 0.405)
DRI+AC	-0.01 (<i>P</i> = 0.686)	0.007 (<i>P</i> = 0.342)

Parameter estimates with respective *P* values are presented. Statistical significance is highlighted in bold. Glaucoma severity only affected the visibility of the anterior LC boundary when Cirrus+EDI was used.

could increase OCT light attenuation thus lowering visibility. However, glaucoma ONHs also exhibit thinner retinal nerve fibre layer and thinner prelaminar tissues, which may mitigate against the attenuating effects of ECM remodelling. This result has important clinical implications as it indicates that morphological studies of the LC performed in normal populations may be readily translatable to glaucoma populations.

The effect of demographic and clinical factors on LC visibility was relatively inconsistent across devices and enhancement techniques and we found no clear associations. A large population is likely needed to establish more convincing associations between LC visibility and various demographic/clinical factors if they exist.

For the visibility of the anterior LC boundary and of the LC insertions, grading agreement between four expert observers was found to be slight to fair. Overall, agreement increased with visibility performance for the LC insertions (all three devices), but decreased with performance for the anterior LC boundary visibility (two of three devices). A likely explanation for this is that the LC insertion grading only has three grades (0–2), whereas there are five for the anterior LC surface (0–4). While addition of EDI and/or AC has the overall effect of increasing the visibility of the anterior LC surface, it is possible that the observers were not necessarily calling these improvements at the same grade or necessarily in the same subjects. The fact that there are five different grades for anterior LC visibility may have led to an increased variability in the calling of grades, whereas the variability post EDI/AC may have been tighter for laminar insertion.

The fact that a subjective grading system was used may be considered a weakness of the study. In a recent study examining the effect of EDI upon LC visibility, a full 3D delineation of the anterior LC surface was carried out.²⁸ While such an approach may seem more valid as it provides a ‘quantifiable’ measure of the relevant region of interest, it is important to remember that manual delineation of LC structures is also entirely subjective. At the time of writing, there is no validated method available for automatically segmenting the LC. Histologic evidence that the posterior surface of the LC is detectable by OCT is awaited; likewise the fidelity of 3D LC morphology as compared to 3D histomorphometric reconstructions has yet to be ascertained. As such, the distillation of the observers’ task of assessing whether or not they felt that portions of the LC were visible is no less valid than asking them to arbitrarily manually delineate the same structures. In essence, we believe that the question ‘do we think we can actually see this structure?’ is more fundamental than ‘what is the distance between these two points?’ and therefore should be addressed as a priority.

TABLE 4. Extended

Spectralis+EDI	Spectralis+AC	Spectralis+EDI+AC	DRI	DRI+AC
0 (<i>P</i> = 0.959)	0 (<i>P</i> = 0.928)	0 (<i>P</i> = 0.669)	0 (<i>P</i> = 0.798)	0 (<i>P</i> = 0.741)
-0.24 (<i>P</i> = 0.248)	0.1 (<i>P</i> = 0.672)	-0.27 (<i>P</i> = 0.193)	-0.02 (<i>P</i> = 0.921)	-0.14 (<i>P</i> = 0.523)
0.25 (<i>P</i> = 0.369)	0.07 (<i>P</i> = 0.822)	0.25 (<i>P</i> = 0.394)	0.15 (<i>P</i> = 0.665)	0.34 (<i>P</i> = 0.275)
-0.2 (<i>P</i> = 0.333)	-0.12 (<i>P</i> = 0.62)	-0.17 (<i>P</i> = 0.409)	-0.38 (<i>P</i> = 0.089)	-0.08 (<i>P</i> = 0.723)
-0.48 (<i>P</i> = 0.104)	0.25 (<i>P</i> = 0.544)	-0.6 (<i>P</i> = 0.133)	-0.4 (<i>P</i> = 0.299)	0.04 (<i>P</i> = 0.933)
-0.02 (<i>P</i> = 0.255)	-0.03 (<i>P</i> = 0.07)	-0.02 (<i>P</i> = 0.142)	0 (<i>P</i> = 0.795)	0 (<i>P</i> = 0.917)
0.06 (<i>P</i> = 0.491)	-0.06 (<i>P</i> = 0.502)	0.01 (<i>P</i> = 0.877)	0.01 (<i>P</i> = 0.927)	-0.03 (<i>P</i> = 0.665)
-0.24 (<i>P</i> = 0.154)	-0.27 (<i>P</i> = 0.109)	-0.12 (<i>P</i> = 0.472)	0 (<i>P</i> = 0.983)	0.18 (<i>P</i> = 0.234)
-0.28 (<i>P</i> = 0.28)	-0.32 (<i>P</i> = 0.201)	-0.09 (<i>P</i> = 0.759)	-0.01 (<i>P</i> = 0.973)	0.5 (<i>P</i> = 0.013)
0 (<i>P</i> = 0.892)	0 (<i>P</i> = 0.402)	0.01 (<i>P</i> = 0.091)	0 (<i>P</i> = 0.856)	0 (<i>P</i> = 0.425)
-0.08 (<i>P</i> = 0.32)	0.15 (<i>P</i> = 0.201)	-0.03 (<i>P</i> = 0.764)	-0.04 (<i>P</i> = 0.615)	0.02 (<i>P</i> = 0.859)
0.01 (<i>P</i> = 0.927)	-0.03 (<i>P</i> = 0.861)	0 (<i>P</i> = 0.983)	-0.16 (<i>P</i> = 0.149)	0.2 (<i>P</i> = 0.204)
0.09 (<i>P</i> = 0.22)	0.04 (<i>P</i> = 0.729)	-0.05 (<i>P</i> = 0.637)	-0.11 (<i>P</i> = 0.194)	0.15 (<i>P</i> = 0.179)
-0.2 (<i>P</i> = 0.045)	0.02 (<i>P</i> = 0.937)	-0.19 (<i>P</i> = 0.35)	-0.08 (<i>P</i> = 0.658)	0.07 (<i>P</i> = 0.707)
-0.01 (<i>P</i> = 0.051)	-0.01 (<i>P</i> = 0.023)	-0.01 (<i>P</i> = 0.112)	-0.01 (<i>P</i> = 0.089)	-0.01 (<i>P</i> = 0.179)
0.02 (<i>P</i> = 0.578)	-0.08 (<i>P</i> = 0.049)	-0.05 (<i>P</i> = 0.167)	0.01 (<i>P</i> = 0.657)	-0.04 (<i>P</i> = 0.275)
-0.05 (<i>P</i> = 0.429)	-0.16 (<i>P</i> = 0.07)	-0.14 (<i>P</i> = 0.115)	-0.06 (<i>P</i> = 0.37)	0 (<i>P</i> = 0.953)
-0.12 (<i>P</i> = 0.121)	-0.15 (<i>P</i> = 0.245)	-0.04 (<i>P</i> = 0.757)	-0.09 (<i>P</i> = 0.375)	0.23 (<i>P</i> = 0.066)

It is also important to note that two of the four expert observers (NGS and MJAG) were directly involved in the development of AC.^{15,21} Although they were masked to patient diagnosis and device, their experience was such that it is possible to identify the EDI and AC images by the improvements in depth penetration. It may be argued that the two expert observers may be biased toward calling higher grades for B-scans assumed to have been applied with AC. We have, however, recently reported quantitative data (using intra- and interlayer contrast measurements) that consistently agree with those reported herein.^{15,21} To further eliminate bias, we have included two additional expert observers (SP and RH) with no prior expertise and experience on AC techniques.

Our privileged position in assessing performance of these three devices, allows us to make direct comparisons among them, which may guide the purchasing decisions of clinicians. Furthermore, the fact that this study has shown a measurable benefit in using the first commercially available SS-OCT device suggests that this method of image acquisition may develop into the predominant technology.

In conclusion, we have investigated the visibility of the LC in healthy and glaucoma patients using three commercially available OCT devices. Overall, our results indicate that AC is superior to EDI in terms of improving LC visibility, although combining EDI with AC generates the optimal visibility. The anterior LC surface is the most consistently detectable feature of the LC, followed by the LC insertions. Posterior LC visibility was generally poor.

Acknowledgments

The authors thank Sun Chen-Hsin, who wrote part of the Java script in ImageJ.

This work was presented in part at the ARVO International Conference, Orlando, Florida, United States, May 2014.

Supported by grants from the Singapore National Eye Centre (Singapore, Singapore); the Ministry of Education; Academic Research Funds; Tier 1 (Singapore, Singapore); an NUS Young Investigator Award (NUSYIA_FY13_P03, R-397-000-174-133; MJAG; Singapore, Singapore); and the UK Department of Health through the award made by the National Institute for Health Research to Moorfields Eye Hospital NHS Foundation Trust and UCL Institute of Ophthalmology for a Biomedical Research Centre for Ophthalmology (NGS; London, UK).

Disclosure: **M.J.A. Girard**, None; **T.A. Tun**, None; **R. Husain**, None; **S. Acharyya**, None; **B.A. Haaland**, None; **X. Wei**, None; **J.M. Mari**, None; **S.A. Perera**, None; **M. Baskaran**, None; **T. Aung**, Carl Zeiss Meditec (F, C, R); **N.G. Strouthidis**, Alcon, Allergan (R), MSD (R), Novartis (R), Heidelberg Engineering (R), Moorfields Pharmaceuticals (S)

References

1. Quigley HA, Addicks EM, Green WR, Maumenee AE. Optic nerve damage in human glaucoma. II. The site of injury and susceptibility to damage. *Arch Ophthalmol*. 1981;99:635-649.
2. Sigal IA, Wang B, Strouthidis NG, Akagi T, Girard MJA. Recent advances in OCT imaging of the lamina cribrosa. *Br J Ophthalmol*. 2014;98:ii34-ii39.
3. Kim TW, Kagemann L, Girard MJ, et al. Imaging of the lamina cribrosa in glaucoma: perspectives of pathogenesis and clinical applications. *Curr Eye Res*. 2013;38:903-909.
4. Girard MJA, Dupps WJ, Mani B, et al. Translating ocular biomechanics into clinical practice: current state and future prospects. *Curr Eye Res*. 2014;40:1-18.
5. Nadler Z, Wang B, Wollstein G, et al. Automated lamina cribrosa microstructural segmentation in optical coherence tomography scans of healthy and glaucomatous eyes. *Biomed Optics Exp*. 2013;4:2596-2608.
6. Park HY, Jeon SH, Park CK. Enhanced depth imaging detects lamina cribrosa thickness differences in normal tension glaucoma and primary open-angle glaucoma. *Ophthalmology*. 2012;119:10-20.
7. Park SC, Kiumehr S, Teng CC, Tello C, Liebmann JM, Ritch R. Horizontal central ridge of the lamina cribrosa and regional differences in laminar insertion in healthy subjects. *Invest Ophthalmol Vis Sci*. 2012;53:1610-1616.
8. Park SC, Hsu AT, Su D, et al. Factors associated with focal lamina cribrosa defects in glaucoma. *Invest Ophthalmol Vis Sci*. 2013;54:8401-8407.
9. Lee EJ, Kim TW, Weinreb RN. Reversal of lamina cribrosa displacement and thickness after trabeculectomy in glaucoma. *Ophthalmology*. 2012;119:1359-1366.
10. Agoumi Y, Sharpe GP, Hutchison DM, Nicoleta MT, Artes PH, Chauhan BC. Laminar and prelaminar tissue displacement during intraocular pressure elevation in glaucoma patients and healthy controls. *Ophthalmology*. 2011;118:53-59.
11. Girard MJ, Strouthidis NG, Desjardins A, Mari JM, Ethier CR. In vivo optic nerve head biomechanics: performance testing of a three-dimensional tracking algorithm. *J R Soc Interface*. 2013;10:20130459.
12. Girard MJA, Zimmo L, White E, Mari JM, Ethier CR, Strouthidis NG. Towards a biomechanically-based diagnosis for glaucoma: in vivo deformation mapping of the human optic nerve head. In: Proceedings of the ASME 2012 Summer Bioengineering Conference; June 20-23, 2012; Fajardo, Puerto Rico, USA; SBC2012-80557.
13. Ren R, Yang H, Gardiner SK, et al. Anterior lamina cribrosa surface depth, age, and visual field sensitivity in the Portland progression project. *Invest Ophthalmol Vis Sci*. 2014;55:1531-1539.
14. Sredar N, Ivers KM, Queener HM, Zouridakis G, Porter J. 3D modeling to characterize lamina cribrosa surface and pore geometries using in vivo images from normal and glaucomatous eyes. *Biomed Optics Exp*. 2013;4:1153-1165.
15. Girard MJ, Strouthidis NG, Ethier CR, Mari JM. Shadow removal and contrast enhancement in optical coherence tomography images of the human optic nerve head. *Invest Ophthalmol Vis Sci*. 2011;52:7738-7748.
16. Ren R, Li B, Gao F, et al. Central corneal thickness, lamina cribrosa and peripapillary scleral histomorphometry in non-glaucomatous Chinese eyes. *Graefes Arch Clin Exp Ophthalmol*. 2010;248:1579-1585.
17. Yang H, Downs JC, Sigal IA, Roberts MD, Thompson H, Burgoyne CF. Deformation of the normal monkey optic nerve head connective tissue following acute IOP elevation within 3-D histomorphometric reconstructions. *Invest Ophthalmol Vis Sci*. 2009;50:5785-5799.
18. Sigal IA, Grimm JL, Jan NJ, Reid K, Minckler DS, Brown DJ. Eye-specific IOP-induced displacements and deformations of human lamina cribrosa. *Invest Ophthalmol Vis Sci*. 2014;55:1-15.
19. Strouthidis NG, Grimm J, Williams GA, Cull GA, Wilson DJ, Burgoyne CF. A comparison of optic nerve head morphology viewed by spectral domain optical coherence tomography and by serial histology. *Invest Ophthalmol Vis Sci*. 51:1464-1474.
20. Park SC, De Moraes CG, Teng CC, Tello C, Liebmann JM, Ritch R. Enhanced depth imaging optical coherence tomography of deep optic nerve complex structures in glaucoma. *Ophthalmology*. 2012;119:3-9.
21. Mari JM, Strouthidis NG, Park SC, Girard MJ. Enhancement of lamina cribrosa visibility in optical coherence tomography images using adaptive compensation. *Invest Ophthalmol Vis Sci*. 2013;54:2238-2247.

22. Hodapp E, Parrish RK II, Anderson DR. *Clinical Decisions in Glaucoma*. St Louis: Mosby; 1993.
23. Copete S, Flores-Moreno I, Montero JA, Duker JS, Ruiz-Moreno JM. Direct comparison of spectral-domain and swept-source OCT in the measurement of choroidal thickness in normal eyes. *Br J Ophthalmol*. 2014;98:334-338.
24. Lee EJ, Kim TW, Kim M, Girard MJ, Mari JM, Weinreb RN. Recent structural alteration of the peripheral lamina cribrosa near the location of disc hemorrhage in glaucoma. *Invest Ophthalmol Vis Sci*. 2014;55:2805-2815.
25. Schneider CA, Rasband WS, Eliceiri KW. NIH image to ImageJ: 25 years of image analysis. *Nat Methods*. 2012;9:671-675.
26. Lee EJ, Kim TW, Weinreb RN, Park KH, Kim SH, Kim DM. Visualization of the lamina cribrosa using enhanced depth imaging spectral-domain optical coherence tomography. *Am J Ophthalmol*. 2011;152:87-95, e81.
27. Miki A, Ikuno Y, Jo Y, Nishida K. Comparison of enhanced depth imaging and high-penetration optical coherence tomography for imaging deep optic nerve head and parapapillary structures. *Clin Ophthalmol (Auckland, NZ)*. 2013;7:1995-2001.
28. Yang H, Qi J, Hardin C, et al. Spectral-domain optical coherence tomography enhanced depth imaging of the normal and glaucomatous nonhuman primate optic nerve head. *Invest Ophthalmol Vis Sci*. 2012;53:394-405.
29. Park HY, Shin HY, Park CK. Imaging the posterior segment of the eye using swept-source optical coherence tomography in myopic glaucoma eyes: comparison with enhanced-depth imaging. *Am J Ophthalmol*. 2014;157:550-557.
30. Park HY, Park CK. Diagnostic capability of lamina cribrosa thickness by enhanced depth imaging and factors affecting thickness in patients with glaucoma. *Ophthalmology*. 2013;120:745-752.
31. Lee EJ, Kim TW, Weinreb RN, Suh MH, Kim H. Lamina cribrosa thickness is not correlated with central corneal thickness or axial length in healthy eyes: central corneal thickness, axial length, and lamina cribrosa thickness. *Graefes Arch Clin Exp Ophthalmol*. 2013;251:847-854.
32. Kim S, Sung KR, Lee JR, Lee KS. Evaluation of lamina cribrosa in pseudoexfoliation syndrome using spectral-domain optical coherence tomography enhanced depth imaging. *Ophthalmology*. 2013;120:1798-1803.
33. Lee EJ, Kim TW, Weinreb RN, et al. Three-dimensional evaluation of the lamina cribrosa using spectral-domain optical coherence tomography in glaucoma. *Invest Ophthalmol Vis Sci*. 2012;53:198-204.
34. Lee EJ, Kim TW, Weinreb RN. Improved reproducibility in measuring the laminar thickness on enhanced depth imaging SD-OCT images using maximum intensity projection. *Invest Ophthalmol Vis Sci*. 2012;53:7576-7582.
35. Yang H, Williams G, Downs JC, et al. Posterior (outward) migration of the lamina cribrosa and early cupping in monkey experimental glaucoma. *Invest Ophthalmol Vis Sci*. 2011;52:7109-7121.
36. Quigley HA, Hohman RM, Addicks EM, Massof RW, Green WR. Morphologic changes in the lamina cribrosa correlated with neural loss in open-angle glaucoma. *Am J Ophthalmol*. 1983;95:673-691.